ACS APPLIED MATERIALS & INTERFACES

Forum Article

Cite This: ACS Appl. Mater. Interfaces XXXX, XXX, XXX−XXX

www.acsami.org

High-Throughput Equilibrium Analysis of Active Materials for Solar Thermochemical Ammonia Synthesis

Christopher J. Bartel,[†] John R. Rumptz,[†,‡] Alan W. Weimer,[†] Aaron M. Holder,[*,†,§] and Charles B. Musgrave[*,†,§,⊥]

[†]Department of Chemical and Biological Engineering and [⊥]Department of Chemistry, University of Colorado, Boulder, Colorado 80309, United States

[§]National Renewable Energy Laboratory, Golden, Colorado 80401, United States

Supporting Information

ABSTRACT: Solar thermochemical ammonia (NH_3) synthesis (STAS) is a potential route to produce NH_3 from air, water, and concentrated sunlight. This process involves the chemical looping of an active redox pair that cycles between a metal nitride and its complementary metal oxide to yield NH_3. To identify promising candidates for STAS cycles, we performed a high-throughput thermodynamic screening of 1,148 metal nitride/metal oxide pairs. This data-driven screening was based on Gibbs energies of crystalline metal oxides and nitrides at elevated temperatures, $G(T)$, calculated using a recently introduced statistically learned descriptor and 0 K DFT formation energies tabulated in the Materials Project database. Using these predicted $G(T)$ values, we assessed the viability of each of the STAS reactions—hydrolysis of the metal nitride, reduction of the metal oxide, and nitrogen fixation to reform the metal nitride—and analyzed a revised cycle that directly converts between metal oxides and nitrides, which alters the thermodynamics of the STAS cycle. For all 1148 redox pairs analyzed and each of the STAS-relevant reactions, we implemented a Gibbs energy minimization scheme to predict the equilibrium composition and yields of the STAS cycle, which reveals new active materials based on B, V, Fe, and Ce that warrant further investigation for their potential to mediate the STAS cycle. This work details a high-throughput approach to assessing the relevant temperature-dependent thermodynamics of thermochemical redox processes that leverages the wealth of publicly available temperature-independent thermodynamic data calculated using DFT. This approach is readily adaptable to discovering optimal materials for targeted thermochemical applications and enabling the predictive synthesis of new compounds using thermally controlled solid-state reactions.

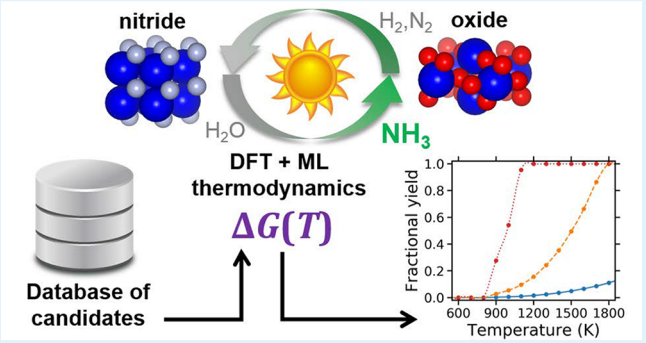

KEYWORDS: *thermochemical ammonia synthesis, chemical looping, high-throughput screening, renewable fuels, reaction engineering*

INTRODUCTION

Developing efficient ammonia (NH_3) synthesis processes that do not emit CO_2 remains a grand challenge for sustainable food, energy, and fuel production.[1−3] NH_3 is industrially produced by the Haber−Bosch process, which is driven by hydrocarbon reforming into H_2 (and CO_2) and catalytically converting H_2 and atmospheric N_2 into NH_3 at high pressure and moderate temperature. Although no CO_2 is directly emitted during the NH_3 synthesis reaction, the scale of centralized production required to make the Haber−Bosch process economically viable requires an immense amount of H_2 input. The large scale of H_2 production required to provide this input is currently only obtained by hydrocarbon reforming, which has resulted in NH_3 production by the Haber−Bosch process accounting for 1−2% of global CO_2 emissions.[4] This motivates the search for an alternative NH_3 synthesis process that either avoids the need for H_2 or operates on the scale of renewable H_2 production technologies to enable globally distributed and renewable NH_3 production.[5,6]

Solar thermochemical water splitting (STWS) leverages the high temperatures (>1500 K) that can be obtained by concentrating solar radiation to produce H_2 from steam at atmospheric pressure without consuming any active material.[7] This is typically achieved by the chemical looping of an active solid, typically a metal oxide (MO) with significant oxygen exchange capacity, such as ceria,[8] perovskite,[9] or hercynite.[10] In one viable approach to STWS, the oxide is partially reduced at high temperature and/or low oxygen partial pressure, generating oxygen vacancies that can then be filled during oxidation by exposure to steam, to yield H_2. In recent years, an

Special Issue: Materials Discovery and Design

Received: January 20, 2019
Accepted: March 12, 2019

DOI: 10.1021/acsami.9b01242
ACS Appl. Mater. Interfaces XXXX, XXX, XXX−XXX

alternative process termed solar thermochemical ammonia synthesis (STAS) was proposed that cyclically converts the active material between a MO and a metal nitride (MN), yielding NH_3 from H_2O and N_2 (Figure 1).[11−13] In this process, NH_3 is formed by the hydrolysis of the MN by steam (600−1200 K), which also converts the nitride into its conjugate oxide. The MO is then reduced at high temperature (1200−1800 K) to metal by a (preferably gaseous) reducing agent. This metal is then used to reduce atmospheric N_2 to reform the metal nitride (600−1200 K) and restart the STAS cycle, which yields NH_3 from H_2O, N_2, and a reducing agent. Although a STAS process that avoids a phase change and is mediated by oxygen vacancies could be proposed, oxygen vacancies likely do not reduce N_2.[14] The phase-change STAS cycle has been previously identified as a technically and economically feasible route to small-scale, renewable NH_3 production.[12]

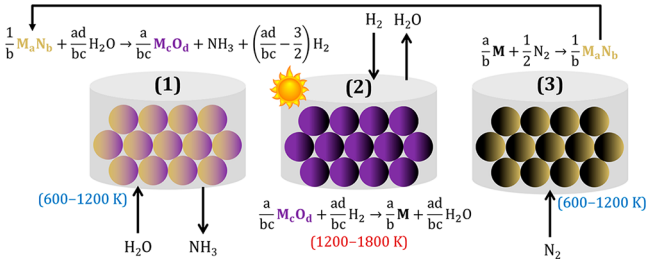

Figure 1. Solar thermochemical ammonia synthesis (STAS) reaction scheme. Reactions are shown on a 1 mol NH_3 per cycle basis. In (1), a metal nitride (M_aN_b) is oxidized by steam to yield a metal oxide (M_cO_d), NH_3, and potentially H_2 (hydrolysis). Note that H_2 can become a necessary reactant for certain MN/MO pairs to achieve the basis of 1 mol NH_3 per cycle. In (2), the metal oxide is reduced by H_2 to yield the metal (M) and steam (reduction). In (3), atmospheric N_2 fixation by the metal yields the metal nitride and closes the STAS cycle. Preferred operating temperatures are provided beside each reactor schematic where concentrated solar radiation drives (2) and integrated heat from this reaction is used to drive (1) and (3).

Unlike most current approaches to STWS, which involve the partial reduction of a single active material, the STAS process studied in this work requires a phase-change from MO to MN. Consequently, the active material is the MO/MN redox pair and the temperature-dependent thermodynamics of these two compounds dictate the viability of a given redox pair for STAS. Prior efforts to identify active materials for STAS have only evaluated ∼35 redox pairs because of the limited number of MNs with experimental Gibbs formation energies, $\Delta G_f(T)$.[15] Recently, we developed a statistically learned descriptor that enables the rapid prediction of $\Delta G_f(T)$ with high accuracy (∼50 meV/atom) for inorganic crystalline solids (e.g., MO and MN) when the standard-state formation enthalpy, ΔH_f, is known.[16] While the number of MNs with tabulated experimental ΔH_f is similarly small, DFT-calculated ΔH_f are available for thousands of MNs and MOs in open materials databases, such as the Materials Project.[17] By integrating the Materials Project data with our high-throughput approach to obtain $\Delta G_f(T)$, we evaluated the thermodynamic viability of 1148 redox pairs made from 354 binary (monometallic) oxides and 197 binary nitrides for the STAS cycle shown in Figure 1. The results of this evaluation provide insight into the thermodynamic and materials challenges associated with each of the STAS reactions and guidance toward which yet-unexplored materials should be the focus of further computational and experimental efforts. Additionally, we present a materials design strategy for coupling open materials databases of 0 K DFT calculated properties with our statistically learned descriptor for $G(T)$ to rapidly assess the thermochemistry of solid-state reactions. This approach has applications for alternative chemical looping processes and for identifying reaction conditions (temperature, precursors, etc.) under which new materials can be synthesized by solid-state thermochemical reactions.

RESULTS AND DISCUSSION

Formation Energies of Redox Pairs. The Gibbs formation energies, $\Delta G_f(T)$, of the oxide and nitride are

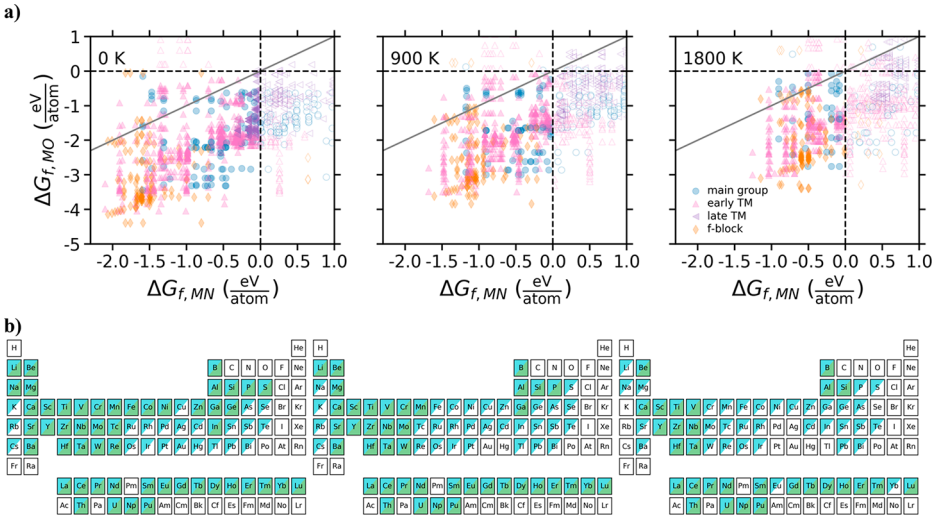

Figure 2. Temperature-dependent Gibbs formation energies of STAS redox pairs: (a) Comparison of the Gibbs formation energies of oxides (MO) and nitrides (MN) for each MN/MO pair in this analysis with temperature increasing from 0 K (left) to 900 K (center) to 1800 K (right). Empty markers correspond with the MO or MN having $\Delta G_f > 0$. The legend for markers by position in the periodic table is provided in the right-most panel. (b) Map of which cations have $\Delta G_{f,MO} < 0$ (top triangle, blue) and $\Delta G_{f,MN} < 0$ (bottom triangle, green) for increasing temperature −0 K (left) to 900 K (center) to 1800 K (right).

DOI: 10.1021/acsami.9b01242
ACS Appl. Mater. Interfaces XXXX, XXX, XXX−XXX

shown as a function of temperature for all 1148 pairs considered in this work (Figure 2a). An essential requirement for the viability of a given pair for STAS is that the solid products at the reaction conditions for each step in the STAS cycle be thermodynamically accessible, i.e., the oxide must be formable at hydrolysis conditions and the nitride must be formable at nitridation conditions. $\Delta G_f(T) < 0$ is a necessary but insufficient requirement for stability. Although stability is ultimately dictated by the decomposition energy,[18,19] in this case, we only plot the formation free energy, $\Delta G_f(T)$, as it provides unique insights into the correlated stabilities of oxides and nitrides, which significantly influences the viability of the STAS process. As Figure 2a illustrates, $\Delta G_{f,MO}(T) < \Delta G_{f,MN}(T)$ for the vast majority of pairs where most $\Delta G_{f,MO}(T)$ values fall below the gray line. Thus, for most pairs, the stability of the nitride dictates the stability of the solid compounds throughout the STAS cycle, i.e., if the nitride is stable, then the oxide will likely also be stable. Because cations have similar affinities for oxygen and nitrogen, the stabilities of nitrides and oxides are correlated with highly stable (unstable) metal oxides typically pairing with highly stable (unstable) metal nitrides.

Temperature has a critical effect on which cations form stable nitrides and oxides (Figure 2b). At 0 K, 831 pairs spanning 51 cations have a nitride and oxide with $\Delta G_f < 0$. However, this decreases substantially at higher temperatures to 566 pairs spanning 41 cations at 900 K and only 387 pairs spanning 29 cations at 1800 K. The cations that yield $\Delta G_{f,MO} < 0$ (blue) and $\Delta G_{f,MN} < 0$ (green) are shown for these temperatures in Figure 2b. Although most of the periodic table appears potentially viable based on a 0 K analysis, because $\Delta G_{f,MN}$(0 K) is near zero for most late transition metals, nitrides composed of these cations have positive $\Delta G_{f,MN}$ even with only modest increases in temperature relative to temperatures more relevant to thermochemical processes (e.g., 900 K). 270 out of 347 oxides (78%) that satisfy the $\Delta G_{f,MO} < 0$ requirement at 0 K also have $\Delta G_{f,MO} < 0$ at 1800 K in contrast to only 59 of 131 nitrides (45%) that meet the $\Delta G_{f,MN} < 0$ criteria. This suggests that temperature swing or the separation of nitrides and oxides during the reaction cycle may be critical to the viability of STAS, i.e., only forming the nitride at low temperature and forming the oxide by exposing this nitride to steam at high temperatures.

Energetics of Each Reaction. The STAS cycles requires the cyclic conversion of nitride to oxide (hydrolysis), oxide to metal (reduction), and metal to nitride (nitrogen fixation). Each reaction is affected uniquely by the formation energies of the oxide and nitride and their dependence on temperature. A thermodynamic assessment of reaction energies for each reaction step helps inform the design principles for identifying a viable redox pair for this process (Figure 3).

The hydrolysis step requires the conversion of water to NH_3 by oxidizing the nitride to its conjugate oxide. Because $\Delta G_{f,NH3} > \Delta G_{f,H2O}$ at all temperatures, this reaction is only spontaneous (reaction energy, $\Delta G_r < 0$) when the conversion of nitride to oxide is thermodynamically favorable in excess of the free energy difference between H_2O and NH_3. Low temperature is also preferred because $\Delta G_r = +337$ kJ/mol NH_3 at 600 K for the conversion of $H_2O$to NH_3 ($1.5H_2O + 0.5N_2 \rightarrow NH_3 + 0.75O_2$), increasing steadily with temperature to 377 kJ/mol NH_3 at 1800 K. At 600 K, 628 pairs meet the requirement that the oxide is sufficiently more stable than the nitride such that $\Delta G_{r,hyd} < 0$ (Figure 3, top). This is expected

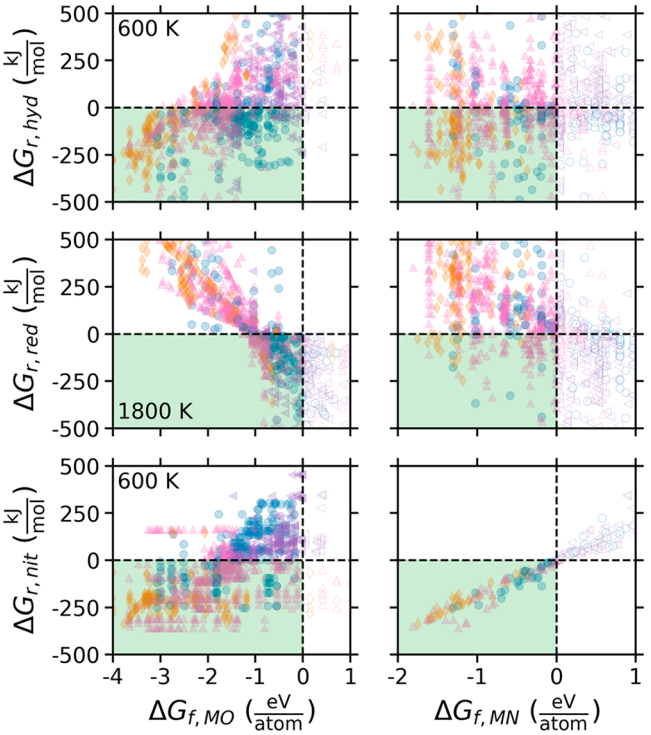

Figure 3. Reaction energies of the STAS cycle. Comparing Gibbs reaction energies to Gibbs formation energies for each reaction in the STAS cycle—hydrolysis (*hyd*, top), oxide reduction (*red*, middle), and nitrogen fixation (*nit*, bottom) — for oxides (left) and nitrides (right). Reaction energies are normalized per mol NH_3 per cycle. Temperatures are shown in the left panel of each reaction and chosen to maximize the number of pairs with $\Delta G_r < 0$. The legend is the same as in the right panel of Figure 2a.

from the results shown in Figure 2a because the oxide typically has a more negative ΔG_f than its corresponding nitride, facilitating the tendency for the nitride to be oxidized by steam and for lattice nitrogens to be replaced by oxygen atoms. Two additional challenges to this reaction have the opposite dependence on temperature. The kinetics of hydrolysis are known to be slow and alleviated by increasing the temperature.[20,21] However, NH_3 is thermodynamically favored to decompose into $N_2 + H_2$ with decreasing ΔG_r (increased driving force for decomposition) as temperature increases, requiring the fast capture and quenching of the liberated NH_3.[22] Although the thermodynamic conversion of nitride to oxide by steam exposure is thermodynamically favorable for ~600 binary redox pairs, these additional kinetic and nonequilibrium challenges will further restrict the number of truly viable pairs for this step.

Once the hydrolysis step has been completed, the difficult challenge of nitrogen fixation to convert the metal oxide back to its typically less stable nitride must begin. The production of metal (e.g., Mg, Fe, etc.) from oxide ore (e.g., MgO, Fe_2O_3, etc.) is responsible for some of the oldest high-temperature industrial processes.[23] However, many of these reductions utilize a solid reducing agent, which complicates cycling for a chemical looping process such as STAS.[24,25] The first redox pair proposed for STAS, AlN/Al_2O_3, required a solid reducing agent (e.g., carbon) to reduce the highly stable oxide Al_2O_3 to Al metal and enable the eventual fixation of atmospheric N_2 to form AlN.[11] The use of gaseous reducing agents, such as H_2, CO, or some combination is preferred to avoid the use of a

DOI: 10.1021/acsami.9b01242
ACS Appl. Mater. Interfaces XXXX, XXX, XXX−XXX

sacrificial reducing agent that must be pelletized with the active materials. In Figure 3 (middle), we show ΔG_r for the reduction of each oxide by H_2 at 1800 K. Although H_2, CO, and CH_4 have comparable reducing powers (and therefore similar thermodynamics of reduction), the carbonaceous reducing agents potentially incorporate carbon into the active materials during reduction and produce CO_2, violating a primary motivation for developing STAS. Thermodynamically, the use of H_2 as reducing agent provides −147 kJ/mol of reducing power due to the oxidation of H_2 to H_2O. Counterintuitive to these processes typically being operated at high temperature, this reducing power increases (becomes more negative) at lower temperature. However, the increase in $\Delta G_{f,MO}$ more than offsets this such that the highest allowed temperature for a given reactor system is preferred for the oxide reduction step. For the oxide reduction by H_2 to be thermodynamically viable, $\Delta G_{f,MO}$ must be > $\Delta G_{f,H2O}$ as illustrated in Figure 3 with a cutoff of approximately −1.2 eV/atom where oxides with $\Delta G_{f,MO}$(1800 K) < −1.2 eV/atom have $\Delta G_{r,red}$(1800 K) > 0. 197 of 438 oxides (54%) meet this condition at the high temperature of 1800 K. It should be noted that 1800 K can be achieved in solar thermochemical systems but presents a number of potential challenges associated with the stability of active and reactor-containment materials that must withstand these conditions for many thousands of cycles.[26] A complication to the requirement that the oxide have only moderately negative ΔG_f is that the nitride will typically have a less negative ΔG_f, frequently becoming >0 for these weakly stable oxides. Temperature swings from high temperatures for oxide reduction to low temperatures for nitride formation can mitigate this issue.

The final reaction of the STAS cycle is the reduction of atmospheric N_2 by the metal to form the metal nitride (Figure 3, bottom). This reaction is the formation reaction for the metal nitride and is thermodynamically preferred at low temperature due to the consumption of gaseous N_2. The 1 mol NH_3 basis used to normalize each pair to one another dictates a nonunity, but still high, correlation between nitrogen fixation ($\Delta G_{r,nit}$) and formation of the metal nitride ($\Delta G_{f,MN}$). Because $\Delta G_{r,nit}$ and $\Delta G_{f,MN}$ are nearly the same property (differing only by the molar coefficients in the reaction), the discussion of $\Delta G_{f,MN}$ in conjunction with Figure 2 also applies to $\Delta G_{r,nit}$, i.e., viable nitride formation reactions become more and more sparse with increasing temperature with the number of binary nitrides having $\Delta G_{f,MN}$ < 0 decreasing from 131 to 59 from 0 to 1800 K. This presents a challenge for the synthesis of metal nitrides from the elemental components (i.e., without elevating the chemical potential of N_2 using, for example, ammonolysis[27]) as the dissociation (reduction) of N_2 on the metal surface has a significant kinetic barrier. This leads to a similar trade-off as with the hydrolysis reaction where the thermodynamics are more favorable when this reaction operates at low temperature, but the kinetic limitations may dictate that the reaction does not proceed at an appreciable rate unless the temperature is elevated.

Limiting Reaction Analysis. Separately analyzing each reaction in the STAS cycle reveals a number of pairs that are viable for each step. However, for the entire STAS cycle to realize equilibrium yields, all reactions must have $\Delta G_r \leq 0$ over some suitable temperature range. This dictates three criteria that must be met by a viable redox pair: (1) the conversion of nitride to oxide must be thermodynamically downhill by more than the thermodynamic penalty of the conversion of H_2O to NH_3 is thermodynamically uphill; (2) H_2O formation must be thermodynamically downhill relative to the formation of the metal oxide ($\Delta G_{f,H2O} < \Delta G_{f,MO}$); and (3) the formation energy of the nitride must be negative ($\Delta G_{f,MN} < 0$). Because the thermodynamics of oxides and nitrides are correlated for a given cation, it is challenging to find a case where all three of these criteria are simultaneously met, and a Sabatier-type phenomena emerges where the interactions between the cation and anion must be significantly strong to favor nitride formation but not so strong that the oxide cannot be reduced by H_2. This volcano-type dependence is visualized in Figure 4

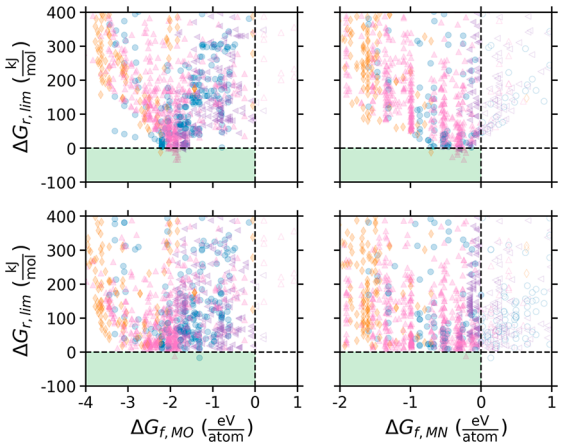

Figure 4. Volcano dependence of STAS energetics. Limiting reaction plot in three- (top) and two-step (bottom) STAS cycles over a maximum allowed temperature swing of 600−1800 K. ΔG_f is shown at 0 K to indicate the target formation enthalpies for each reactant that dictates the minimum of the volcano.

(top panel) and pairs based on Mn, Fe, W, Tc, and Yb are the only ones that lie in the favorable region where $\Delta G_{r,lim}$ < 0. Notably, Mn-based oxides and nitrides were recently demonstrated as a promising system for STAS.[28] The volcano plot reveals an apparent optimal formation energy for the oxide and nitride in the redox pair with $\Delta G_{f,MO}$(0 K) ∼ −2 eV/atom and $\Delta G_{f,MN}$(0 K) ∼ −0.5 eV/atom minimizing the limiting ΔG_r for the cycle. Importantly, a number of pairs have $\Delta G_{r,lim}$ only slightly larger than 0 and these can still be effective active materials for STAS, although they will yield <1 mol NH_3 per cycle. For comparison, the maximum yield of H_2 for one vacancy-mediated STWS cycle is the number of oxygen vacancies that can be thermally generated in the oxide, typically much less than 1 mol/mol MO. Additionally, this work is focused only on binary (monometallic) redox pairs as an initial screening, yet binary compounds account for only ∼13% of the compounds in the Materials Project database, suggesting that ample opportunity may exist to design redox pairs based on oxides and nitrides composed of multiple cations.

The volcano-type dependence of the limiting reaction energy on the active material formation energies can be averted by considering a two-step instead of a three-step cycle where the oxide is directly converted to its corresponding nitride by its simultaneous exposure to a reducing agent and N_2 (Figure 4, bottom panel), for example, where H_2 is used as the reducing agent:

$$\frac{a}{bc}M_cO_d + \frac{ad}{bc}H_2 + \frac{1}{2}N_2 \rightarrow \frac{1}{b}M_aN_b + \frac{ad}{bc}H_2O \qquad (4)$$

DOI: 10.1021/acsami.9b01242
ACS Appl. Mater. Interfaces XXXX, XXX, XXX−XXX

This approach was utilized previously in STAS with methane as a reducing agent[28] and this reaction is analogous to the ammonolysis of metal oxides which has been used extensively for nitride synthesis.[27] The two-step cycle is the hydrolysis reaction (eq 1 in Figure 1) and the reverse of this reaction (eq 4), replacing NH_3 with H_2 + N_2, so that NH_3 is still produced in each cycle. In this way, the significantly positive $\Delta G_{f,NH3}$ does not facilitate the transformation of oxide to nitride as in ammonolysis and appears only as a product during hydrolysis. The hydrolysis reaction is rarely thermodynamically challenging because it involves the typically downhill conversion of nitride to oxide (Figure 3). However, the direct formation of nitride from the oxide is the thermodynamically problematic reaction. Because the oxide and nitride are present during both reactions, there is no longer a volcano-type dependence of $\Delta G_{r,lim}$ on ΔG_f and the relative formation energies of the oxide and nitride are more indicative of $\Delta G_{r,lim}$. In addition to altering the thermodynamic considerations of the STAS cycle, the two-step cycle minimizes the number of reaction steps and eliminates the need to handle a pure metal, which may be prone to sintering, melting, or sublimating at elevated temperatures. However, only pairs based on Na, Fe, and Tc (an unlikely candidate) appear in the viable region where $\Delta G_r < 0$ for both reactions over the temperature range of 600−1800 K.

Equilibrium Product Distributions. Although instructive, the determination of viable pairs by the limiting reaction energy analysis shown in Figure 4 is not exhaustive because it takes a pairwise approach to each reaction. That is, it considers only each of the reactions as written in Figure 1 when, in reality, a number of chemical transformations could occur for a given set of reactants and reaction conditions. For instance, many of these pairs are complicated by the existence of alternative oxide and nitride phases that are thermodynamically more favorable than the solids of the particular pair. Ascertaining which of the pairs are truly thermodynamically viable for STAS requires an equilibrium analysis by Gibbs energy minimization, which determines the molar composition that minimizes the combined free energy of an allowed set of species.[29] In this approach, an initial feed of reactants is dictated by the stoichiometry of the pair and allowed to reach equilibrium with a given set of species at some temperature under the constraint of molar conservation and with the objective of minimizing the Gibbs energy function. This approach enables the determination of which oxides and nitrides are favored to form at a given set of reaction conditions. As an example, W_2N_3/W_2O_5 appears thermodynamically viable from the limiting reaction analysis for the three-step cycle, but neither the oxide nor the nitride are the thermodynamically favored oxide or nitride of tungsten (Figure 5). Instead, the hydrolysis of W_2N_3 yields only WO_3 and not W_2O_5 and the nitridation of W forms WN_2. This limits the viability of W as a metal reactant because WO_3 is not as readily reduced to W in the presence of H_2.

Repeating this analysis for all reactions and all pairs produces the yield plots shown in Figure 6 which emphasizes the difficult trade-off that must be achieved between the oxide and nitride of the redox pair. In Figure 6 (left), the two reactions which comprise the two-step cycle are compared—hydrolysis, *hyd*, and the combined reduction of the oxide and formation of the nitride, *redN*. The vast majority of points lie along the *x*- or *y*-axis, indicating ∼0 yield for one of the involved reactions. Only 5 of 1148 pairs have Y_{hyd} and Y_{redN} > 0.01 given a maximum allowed temperature swing of 600−1800 K: BN/B_2O_3, VN/VO_2, Tc_3N/TcO_2, CeN/Ce_7O_{12}, and PuN/Pu_2O_3. The pairs based on Tc and Pu are not practical because of their scarcity and radioactivity, leaving B, V, and Ce as cations with significant promise for the two-step cycle based on this thermodynamic analysis.

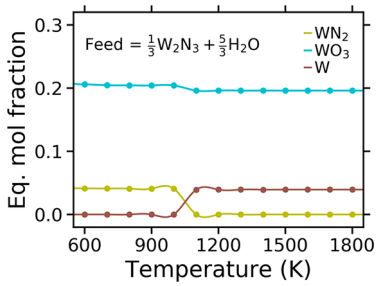

Figure 5. Predicted yields for tungsten nitride hydrolysis. Equilibrium product distribution predicted by Gibbs energy minimization for the hydrolysis of WN_2. The feed considered for each reaction is dictated by the equations shown in Figure 1. This results in feeds of 1/3 mol WN_2 + 5/3 mol H_2O for hydrolysis.

The three-step cycle requires the careful balance of hydrolysis, reduction and nitride formation, shown in the second through fourth panels of Figure 6. Although each pairwise combination of reactions show a number of pairs with high yields for both reactions (i.e., points away from the axes), there are only 5 of 1148 pairs that exhibit Y_{hyd}, Y_{red}, and Y_{nit} all >0.01 over the same allowed temperature swing of 600−1800 K: P_3N_5/P_2O_5, GaN/Ga_2O_3, Tc_3N/TcO_2, FeN/FeO, and FeN/Fe_3O_4. Tc is again not preferred because of its scarcity. P and Ga are problematic for the three-step cycle because of the low melting points of their elemental phases (∼300 K), leaving Fe as the only metal reactant with significant promise based on this thermodynamic assessment.

Shifting Equilibrium. In addition to temperature, the partial pressure of reactant and product species is an important parameter for dictating the thermodynamics of each reaction. For STWS, controlling the partial pressures of H_2O during oxidation (by excess steam feed) and O_2 during reduction (by inert gas sweep) was shown to enable isothermal H_2 production using hercynite as an active material.[30] For STAS, the reduction (or simultaneous reduction and nitridation) of the metal oxide is the logical step to target that could benefit from manipulations of partial pressure by considering operation in the regime where the partial pressure of H_2O is decreased relative to the partial pressure of H_2. This can be achieved by exposing the metal oxide to greater-than-equilibrium amounts of H_2. Considering 100⊆ excess of H_2 increases the yields of eight pairs to >0.1 mol NH_3/cycle, three of which were previously identified as having >0.01 yield at equilibrium reactant amounts—BN/B_2O_3, VN/VO_2, and FeN/Fe_3O_4—and five additional pairs—CrN/Cr_2O_3, MoN/MoO_2, WN_2/WO_3,MnN/MnO, and Mn_2N/MnO. Notably, STAS cycles based on Cr, Mo, and Mn have been previously investigated with varying degrees of success.[6,28,31,32] For the reverse reaction that occurs during STWS, water splitting over a reduced metal oxide to produce H_2, similar ratios (100⊆ the equilibrium amount of H_2O) were used to drive equilibrium toward H_2 production, which led to increases in solar-to-hydrogen efficiencies for the overall cycle.[33] The yet-unexplored pairs based on Fe and V show significant promise as their yields per cycle are increased substantially by considering

DOI: 10.1021/acsami.9b01242
ACS Appl. Mater. Interfaces XXXX, XXX, XXX−XXX

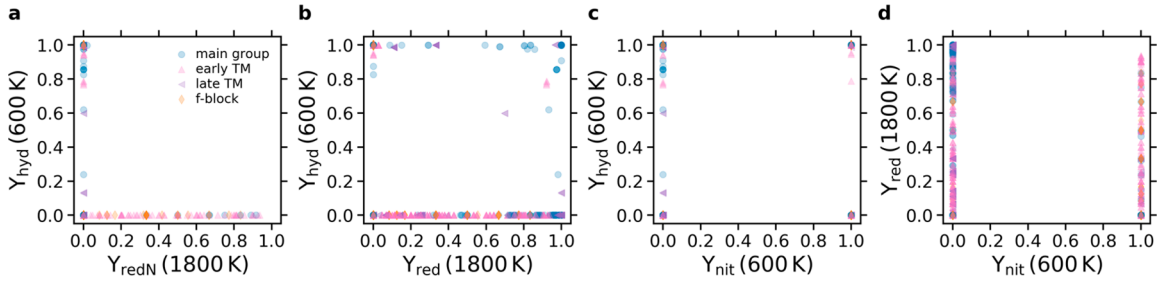

Figure 6. Reaction-wise equilibrium yields for all pairs. Yields of each reaction in the two- and three-step cycles. (a) All reactions for the two-step cycle: hydrolysis, *hyd*, and nitride formation from the oxide, *redN*. (b) Hydrolysis and oxide reduction by H_2, *red*. (c) Hydrolysis and nitride formation from the metal, *nit*. (d) Reduction and nitride formation from the metal.

only 10⊆ (instead of 100⊆) the equilibrium amount of H_2 feed. The effects of excess H_2 for the reduction of Fe_3O_4 to Fe and the formation of VN from VO_2 are shown in Figure 7. This

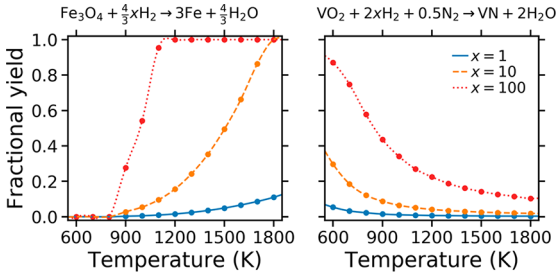

Figure 7. Increasing yields by shifting equilibrium. Left: yield of Fe from the reduction of Fe_3O_4 as a function of the number of moles of H_2 fed. Right: yield of VN for the reaction of VO_2 with H_2 and N_2 as a function of the number of H_2 moles in the feed. Note that neither the direct reduction of VO_2 nor the reduction of Fe_3O_4 in the presence of N_2 have appreciable yields at any T or x evaluated.

introduces an additional parameter that can be varied to optimize the thermodynamics of these reactions but also introduces a processing challenge associated with separating and heating the excess gas.

Nonequilibrium Considerations. Along with thermodynamics, the kinetics of each reaction in STAS are critical to the viability of the NH_3 synthesis process, especially for reactions involving nitrogen. The corrosion of metal nitrides by H_2O is a kinetically limited process for many nitrides below 1200 K, primarily associated with the need to break metal−nitrogen bonds that can have significant covalent character.[20,21,34] Similarly, the reduction of N_2 for metal nitride synthesis requires the activation and cleavage of the triply bonded N_2 molecule, which also poses a significant kinetic challenge. The difficulty in reducing N_2 can result in metals becoming only partially nitridated, limiting the NH_3 yield that can be achieved on a per cycle basis, as this quantity is directly linked with the amount N_2 that can be fixed to the metal. Conversely, the strongly bound metal nitride species can be advantageous compared with what is captured in this equilibrium analysis because of the high metastability of metal nitrides compared with other compounds.[16,35,36] That is, there are likely nitrides that will not appear in a Gibbs energy minimization analysis that are still realized experimentally because of the prevalence of metastable (nonequilibrium) nitride species. Although the presumption of equilibrium is a significant approximation, these results do indicate the challenges associated with each reaction and which active materials show promise for engineering into viable materials for this process.

CONCLUSIONS

Solar thermochemical ammonia synthesis (STAS) is a potential route to producing NH_3 from air, water, and concentrated sunlight. In this work, we utilized the Materials Project database of density functional theory calculations and a recently introduced descriptor for the Gibbs energy of compounds to screen the thermodynamic viability of 1148 metal nitride/metal oxide redox pairs for this process. Using the resulting thermochemical data, we established thermodynamic rationale for the viability of each reaction in the STAS cycle—hydrolysis of the nitride to oxide (NH_3 synthesis), reduction of the oxide by H_2, and formation of the metal nitride from atmospheric nitrogen. Taking these reactions together, we identified a volcano-type dependence of the limiting Gibbs energy of reaction over the cycle with respect to the formation energy of the nitride and oxide. By considering an alternative cycle with just two reactions, hydrolysis and the direct formation of the nitride from the oxide, this volcano-type dependence can be removed and the limiting reaction energy depends instead on the relative stabilities of the oxide and nitride. Going beyond reaction energies, we performed a Gibbs energy minimization analysis for all 1148 pairs and each of the four STAS-relevant reactions to generate a predicted reaction equilibrium product distribution and quantify the yields of each reaction for each pair. This analysis reveals pairs based on B, V, Fe, and Ce as yielding >0.01 mol NH_3 per cycle given equilibrium feeds for each reaction, none of which have been previously studied for STAS. The effects of shifting equilibrium by feeding excess reactant was also studied. This effect reproduces the viability of previously studied pairs based on Cr, Mo, and Mn, indicates the viability of a yet-unexplored pair based on W, and enhances the predicted yields of pairs based on V and Fe.

Importantly, this work focused exclusively on binary (monometallic) active materials, yet these compounds comprise only ∼10% of known materials. Therefore, these results indicate cations that should form the basis of more complex materials (i.e., ternary and quaternary compounds) and establish key thermodynamic considerations for the STAS cycle. It is also plausible that the total conversion between oxide and nitride, as studied here, is not necessarily required and mixed-anion, M(O,N,H), species may have more desirable thermodynamics for any given step. Additionally, active materials with multiple anions potentially enables additional thermodynamic handles for encouraging desired phase changes

DOI: 10.1021/acsami.9b01242
ACS Appl. Mater. Interfaces XXXX, XXX, XXX−XXX

by the control of the chemical potential (partial pressure) of each anion in the gas phase.

The thermodynamic screening approach used here is also readily adaptable to arbitrary thermochemical reactions and can be used to guide the synthesis of new materials or the identification of active materials for other redox processes. For example, the equilibrium yields for an arbitrary solid-state synthesis reaction from solid precursors in a specified atmosphere can be readily predicted using the methods described in this work. By coupling the vast availability of 0 K DFT calculations provided in open materials databases with a high-throughput descriptor for the temperature-dependent solid-state thermodynamics, we overcome the sparsity of temperature-dependent thermodynamics available for solid compounds obtained experimentally or computed directly using quantum chemical approaches.

In summary, a thermodynamic assessment of 1148 candidate active materials for solar thermochemical ammonia synthesis highlights the challenges of finding active materials for this process. This cycle requires a careful balance between the stability of metal nitrides and metal oxides that share the same metal as the metal must bind nitrogen strongly enough to form the metal nitride, but not so strongly that the metal oxide cannot be reduced. By evaluating a broad space of candidates, we identify active materials containing B, V, Fe, and Ce as the most promising materials for future additional computational and experimental evaluation (see the Supporting Information for more details on the newly identified candidates). Even the most promising monometallic candidates are predicted to have relatively low yields of NH_3 per cycle, which motivates future work to explore how the incorporation of multiple cations or anions may improve the performance of these materials for this process.

METHODS

Formation enthalpies and structures were retrieved for all binary nitrides and oxides in the Materials Project with <20 atoms in the formula unit (to avoid including defect structures), excluding azides and peroxides (due to their instability) and compounds with H, C, N, O, F, Cl, Br, I as cations (because they are unlikely to be solid at relevant temperatures).

All reported Gibbs formation energies, ΔG_f, of solid compounds were obtained using eqs 5-7.ΔG_f of nonsolids (H_2, N_2, H_2O, NH_3) were obtained from FactSage.[37]

$$\Delta G_f(0\ \mathrm{K}) = \Delta H_f(0\ \mathrm{K}) \tag{5}$$

$$\Delta G_f(T > 0\ \mathrm{K}) = \Delta H_f(0\ \mathrm{K}) + G^{\delta}(T) - \sum_i^N \alpha_i G_i(T) \tag{6}$$

$$G^{\delta}(T) = (-2.48 \times 10^{-4} \cdot \ln(V) - 8.94 \times 10^{-5}\ \mathrm{mV}^{-1})T + 0.181\ln(T) - 0.882 \tag{7}$$

ΔH_f is the formation energy retrieved from the Materials Project database. G^{δ} (eV/atom) is the descriptor described in ref 16. which depends on the DFT-calculated atomic volume (V, Å^3/atom), the reduced atomic mass (m, amu), and temperature (T, K). α_i is the stoichiometric weight of element α_i in the compound, and G_i is the Gibbs free energy of element, i.

The prediction of ΔG_f using eqs 5-7 for a wide range of 440 inorganic crystalline solids is described in detail in ref 16. As only metal nitrides and metal oxides are pertinent to this work, we also assessed the performance of this method specifically on these compounds. The data set used in ref 16 includes 31 metal nitrides [20 with experimentally obtained[37] $G(T)$ and 11 with computationally obtained[38] $G(T)$ using the quasiharmonic approximation] and 104 metal oxides [69 with experimentally obtained $G(T)$ and 35 with computationally obtained $G(T)$ using the quasiharmonic approximation]. For the nitrides, there are 353 (T, G) data points for these 31 compounds and the mean absolute difference (MAD) between the descriptor and the validation source (experiment or the quasiharmonic approximation) is 47 meV/atom. For the oxides, there are 1,230 (T, G) data points for these 104 compounds and the MAD = 42 meV/atom. Restricting the comparison to only experimental data as a validation source reduces the MAD to 44 meV/atom and 37 meV/atom for the nitrides and oxides, respectively. In both cases, these accuracies are comparable to those reported for the full set of 440 materials studied in ref 16. In all applications of the descriptor—predicted formation energies, reaction energies, or equilibrium product distributions—the accuracy of the $G(T)$ prediction dictates the efficacy of these approaches and these results provide confidence that the descriptor has sufficient accuracy for the compounds of interest.

Gibbs reaction energies, ΔG_r were calculated as the stoichiometrically weighted difference between Gibbs formation energies for the products and reactants of each reaction in the STAS cycle:

$$\Delta G_r(T) = \sum_i^{\text{products}} \nu_i \Delta G_{f,i}(T) - \sum_i^{\text{reactants}} \nu_i \Delta G_{f,i}(T) \tag{8}$$

where ν_i is the coefficient of species i that dictates 1 mol NH_3 generated per cycle at equilibrium (eqs 1−3 in Figure 1 and eq 4).

The Gibbs energy minimization approach used to determine equilibrium product distributions and yields was adapted from ref 29. The Gibbs energy of the system, G, is the sum of the product of molar compositions, x_i, and molar Gibbs energies, g_i, over N species in equilibrium:

$$G = \sum_i^N x_i g_i \tag{9}$$

where the molar Gibbs energies, g_i, are taken to be the Gibbs formation energies, $\Delta G_{f,i}$ modified by the activities, a_i. $\Delta G_{f,i}$ is obtained from eqs 5−7 for solid species and FactSage for nonsolid species. R is the gas constant and T is the temperature:

$$g_i = \Delta G_{f,i}(T) + RT\ln a_i \tag{10}$$

The activity of solid phases is taken to be 1. The activity of gas phases is taken to be the partial pressure, p_i:

$$a_i = \begin{Bmatrix} 1 \text{ if solid} \\ p_i \text{ if gas} \end{Bmatrix} \tag{11}$$

The partial pressure is determined as the product of the number of moles of a certain gaseous species, n_i, and the total pressure, P (set to 1 atm in this work), divided by the number of moles of gas in the system, n^g:

$$p_i = \frac{n_i}{n^g} P \tag{12}$$

$$n^g = \sum_i^m x_i \text{ for } m \text{ gaseous species} \tag{13}$$

Using a molar basis, the Gibbs function thus becomes

$$G = \sum_i^m x_i \left[\Delta G_{f,i}(T) + RT\ln\left(\frac{x_i}{\sum_i^m x_i} \right) \right] + \sum_i^{N-m} x_i \Delta G_{f,i}(T) \tag{14}$$

for m gaseous species and N-m solid species. G is then minimized subject to the constraint of molar conservation:

$$\sum_i^N \alpha_{ij} x_i = b_j \tag{15}$$

DOI: 10.1021/acsami.9b01242
ACS Appl. Mater. Interfaces XXXX, XXX, XXX−XXX

where α_{ij} is the number of moles of element, j, in species i and b_j is the number of moles of element j in the feed. b_j is dictated for each reaction by eqs 1-4 which yield 1 mol NH_3 per cycle if ΔG_r for all reactions = 0 (the equilibrium constants are equal to 1). The molar NH_3 basis controls for the effects of metal-to-oxygen and metal-to-nitrogen ratios in the active materials.

A more detailed description of the Methods is provided in Figure S1 and the corresponding discussion in the Supporting Information.

■ ASSOCIATED CONTENT

Supporting Information

The Supporting Information is available free of charge on the ACS Publications website at DOI: 10.1021/acsami.9b01242.

Detailed description of analysis workflow, table of newly identified candidates, and equilibrium product distributions and yields for newly identified candidates (PDF)

■ AUTHOR INFORMATION

Corresponding Authors

*Email: aaron.holder@colorado.edu.

*Email: charles.musgrave@colorado.edu.

ORCID

Aaron M. Holder: 0000-0002-1878-1541

Charles B. Musgrave: 0000-0002-5732-3180

Present Address

‡J.R.R. Department of Chemical Engineering, University of Washington, Seattle, Washington 98195, USA

Notes

The authors declare no competing financial interest.

■ ACKNOWLEDGMENTS

The authors thank Ann Deml for early ideas and discussions related to this work and Samantha Millican for helpful context regarding solar thermochemical water splitting. This work was supported by the National Science Foundation (Awards CBET-1806079 and CHE-1800592) and the U.S. Department of Energy, and Fuel Cell Technologies Office (Award DE-EE0008088).

■ REFERENCES

(1) Chen, J. G.; Crooks, R. M.; Seefeldt, L. C.; Bren, K. L.; Bullock, R. M.; Darensbourg, M. Y.; Holland, P. L.; Hoffman, B.; Janik, M. J.; Jones, A. K.; Kanatzidis, M. G.; King, P.; Lancaster, K. M.; Lymar, S. V.; Pfromm, P.; Schneider, W. F.; Schrock, R. R. Beyond fossil fuel–driven nitrogen transformations. *Science* **2018**, *360* (6391), eaar6611.

(2) Wang, L.; Xia, M.; Wang, H.; Huang, K.; Qian, C.; Maravelias, C. T.; Ozin, G. A. Greening Ammonia toward the Solar Ammonia Refinery. *Joule* **2018**, *2* (6), 1055–1074.

(3) Pfromm, P. H. Towards sustainable agriculture: Fossil-free ammonia. *J. Renewable Sustainable Energy* **2017**, *9* (3), 034702.

(4) Service, R. Ammonia—a renewable fuel made from sun, air, and water—could power the globe without carbon. *Science* 2018.

(5) McEnaney, J. M.; Singh, A. R.; Schwalbe, J. A.; Kibsgaard, J.; Lin, J. C.; Cargnello, M.; Jaramillo, T. F.; Nørskov, J. K. Ammonia synthesis from N2 and H2O using a lithium cycling electrification strategy at atmospheric pressure. *Energy Environ. Sci.* **2017**, *10* (7), 1621–1630.

(6) Michalsky, R.; Avram, A. M.; Peterson, B. A.; Pfromm, P. H.; Peterson, A. A. Chemical looping of metal nitride catalysts: low-pressure ammonia synthesis for energy storage. *Chemical Science* **2015**, *6* (7), 3965–3974.

(7) Muhich, C. L.; Ehrhart, B. D.; Al-Shankiti, I.; Ward, B. J.; Musgrave, C. B.; Weimer, A. W. A review and perspective of efficient hydrogen generation via solar thermal water splitting. *Wiley Interdisciplinary Reviews: Energy and Environment* **2016**, *5* (3), 261–287.

(8) Chueh, W. C.; Falter, C.; Abbott, M.; Scipio, D.; Furler, P.; Haile, S. M.; Steinfeld, A. High-Flux Solar-Driven Thermochemical Dissociation of CO_2 and H_2O Using Nonstoichiometric Ceria. *Science* **2010**, *330* (6012), 1797–1801.

(9) McDaniel, A. H.; Miller, E. C.; Arifin, D.; Ambrosini, A.; Coker, E. N.; O'Hayre, R.; Chueh, W. C.; Tong, J. Sr- and Mn-doped LaAlO3−δ for solar thermochemical H2 and CO production. *Energy Environ. Sci.* **2013**, *6* (8), 2424–2428.

(10) Muhich, C. L.; Ehrhart, B. D.; Witte, V. A.; Miller, S. L.; Coker, E. N.; Musgrave, C. B.; Weimer, A. W. Predicting the solar thermochemical water splitting ability and reaction mechanism of metal oxides: a case study of the hercynite family of water splitting cycles. *Energy Environ. Sci.* **2015**, *8* (12), 3687–3699.

(11) Gálvez, M. E.; Halmann, M.; Steinfeld, A. Ammonia Production via a Two-Step Al2O3/AlN Thermochemical Cycle. 1. Thermodynamic, Environmental, and Economic Analyses. *Ind. Eng. Chem. Res.* **2007**, *46* (7), 2042–2046.

(12) Michalsky, R.; Parman, B. J.; Amanor-Boadu, V.; Pfromm, P. H. Solar thermochemical production of ammonia from water, air and sunlight: Thermodynamic and economic analyses. *Energy* **2012**, *42* (1), 251–260.

(13) Gao, Y.; Wu, Y.; Zhang, Q.; Chen, X.; Jiang, G.; Liu, D. N-desorption or NH3 generation of TiO2-loaded Al-based nitrogen carrier during chemical looping ammonia generation technology. *Int. J. Hydrogen Energy* **2018**, *43*, 16589.

(14) Michalsky, R.; Steinfeld, A. Computational screening of perovskite redox materials for solar thermochemical ammonia synthesis from N2 and H2O. *Catal. Today* **2017**, *286*, 124–130.

(15) Michalsky, R.; Pfromm, P. H. Thermodynamics of metal reactants for ammonia synthesis from steam, nitrogen and biomass at atmospheric pressure. *AIChE J.* **2012**, *58* (10), 3203–3213.

(16) Bartel, C. J.; Millican, S. L.; Deml, A. M.; Rumptz, J. R.; Tumas, W.; Weimer, A. W.; Lany, S.; Stevanović, V.; Musgrave, C. B.; Holder, A. M. Physical descriptor for the Gibbs energy of inorganic crystalline solids and temperature-dependent materials chemistry. *Nat. Commun.* **2018**, *9* (1), 4168.

(17) Jain, A.; Ong, S. P.; Hautier, G.; Chen, W.; Richards, W. D.; Dacek, S.; Cholia, S.; Gunter, D.; Skinner, D.; Ceder, G.; Persson, K. A. Commentary: The Materials Project: A materials genome approach to accelerating materials innovation. *APL Mater.* **2013**, *1* (1), 011002.

(18) Zunger, A. Inverse design in search of materials with target functionalities. *Nature Reviews Chemistry* **2018**, *2*, 0121.

(19) Bartel, C. J.; Weimer, A. W.; Lany, S.; Musgrave, C. B.; Holder, A. M. The role of decomposition reactions in assessing first-principles predictions of solid stability. *npj Computational Materials* **2019**, *5* (1), 4.

(20) Bartel, C. J.; Muhich, C. L.; Weimer, A. W.; Musgrave, C. B. Aluminum Nitride Hydrolysis Enabled by Hydroxyl-Mediated Surface Proton Hopping. *ACS Appl. Mater. Interfaces* **2016**, *8* (28), 18550–18559.

(21) Michalsky, R.; Pfromm, P. H. An Ionicity Rationale to Design Solid phase Metal Nitride Reactants for Solar Ammonia Production. *J. Phys. Chem. C* **2012**, *116* (44), 23243–23251.

(22) White, A. H.; Melville, W. THE DECOMPOSITION OF AMMONIA AT HIGH TEMPERATURES. *J. Am. Chem. Soc.* **1905**, *27* (4), 373–386.

(23) Taylor, G. B.; Starkweather, H. W. REDUCTION OF METAL OXIDES BY HYDROGEN. *J. Am. Chem. Soc.* **1930**, *52* (6), 2314–2325.

(24) Halmann, M.; Frei, A.; Steinfeld, A. Magnesium Production by the Pidgeon Process Involving Dolomite Calcination and MgO Silicothermic Reduction: Thermodynamic and Environmental Analyses. *Ind. Eng. Chem. Res.* **2008**, *47* (7), 2146–2154.

(25) Chubukov, B. A.; Palumbo, A. W.; Rowe, S. C.; Wallace, M. A.; Weimer, A. W. Enhancing the Rate of Magnesium Oxide Carbothermal Reduction by Catalysis, Milling, and Vacuum Operation. *Ind. Eng. Chem. Res.* **2017**, *56* (46), 13602–13609.

DOI: 10.1021/acsami.9b01242
ACS Appl. Mater. Interfaces XXXX, XXX, XXX–XXX

(26) Roeb, M.; Neises, M.; Monnerie, N.; Call, F.; Simon, H.; Sattler, C.; Schmücker, M.; Pitz-Paal, R. Materials-Related Aspects of Thermochemical Water and Carbon Dioxide Splitting: A Review. *Materials* **2012**, *5* (11), 2015.
(27) Elder, S. H.; DiSalvo, F. J.; Topor, L.; Navrotsky, A. Thermodynamics of ternary nitride formation by ammonolysis: application to lithium molybdenum nitride (LiMoN2), sodium tungsten nitride (Na3WN3), and sodium tungsten oxide nitride (Na3WO3N). *Chem. Mater.* **1993**, *5* (10), 1545−1553.
(28) Heidlage, M. G.; Kezar, E. A.; Snow, K. C.; Pfromm, P. H. Thermochemical Synthesis of Ammonia and Syngas from Natural Gas at Atmospheric Pressure. *Ind. Eng. Chem. Res.* **2017**, *56* (47), 14014−14024.
(29) Eriksson, G. Thermodynamic Studies of High Temperature Equilibria. *Acta Chem. Scand.* **1971**, *25*, 2651−2658.
(30) Muhich, C. L.; Evanko, B. W.; Weston, K. C.; Lichty, P.; Liang, X.; Martinek, J.; Musgrave, C. B.; Weimer, A. W. Efficient Generation of H_2 by Splitting Water with an Isothermal Redox Cycle. *Science* **2013**, *341* (6145), 540.
(31) Michalsky, R.; Pfromm, P. H. Chromium as reactant for solar thermochemical synthesis of ammonia from steam, nitrogen, and biomass at atmospheric pressure. *Sol. Energy* **2011**, *85* (11), 2642−2654.
(32) Michalsky, R.; Pfromm, P. H.; Steinfeld, A. Rational design of metal nitride redox materials for solar-driven ammonia synthesis. *Interface Focus* **2015**, *5* (3), 20140084.
(33) Scheffe, J. R.; Weibel, D.; Steinfeld, A. Lanthanum−Strontium−Manganese Perovskites as Redox Materials for Solar Thermochemical Splitting of H2O and CO2. *Energy Fuels* **2013**, *27* (8), 4250−4257.
(34) Sun, W.; Bartel, C. J.; Arca, E.; Bauers, S.; Matthews, B.; Orvananos, B.; Chen, B.-R.; Toney, M. F.; Schelhas, L. T.; Tumas, W.; Tate, J.; Zakutayev, A.; Lany, S.; Holder, A.; Ceder, G., A Map of the Inorganic Ternary Metal Nitrides. *ArXiv Prepr.* at https://arxiv.org/abs/1809.09202 **2018**.
(35) Sun, W.; Holder, A.; Orvañanos, B.; Arca, E.; Zakutayev, A.; Lany, S.; Ceder, G. Thermodynamic Routes to Novel Metastable Nitrogen-Rich Nitrides. *Chem. Mater.* **2017**, *29* (16), 6936−6946.
(36) Sun, W.; Dacek, S. T.; Ong, S. P.; Hautier, G.; Jain, A.; Richards, W. D.; Gamst, A. C.; Persson, K. A.; Ceder, G. The thermodynamic scale of inorganic crystalline metastability. *Sci. Adv.* **2016**, *2* (11), e1600225.
(37) Bale, C. W.; Bélisle, E.; Chartrand, P.; Decterov, S. A.; Eriksson, G.; Gheribi, A. E.; Hack, K.; Jung, I. H.; Kang, Y. B.; Melançon, J.; Pelton, A. D.; Petersen, S.; Robelin, C.; Sangster, J.; Spencer, P.; Van Ende, M. A. FactSage thermochemical software and databases, 2010−2016. *CALPHAD: Comput. Coupling Phase Diagrams Thermochem.* **2016**, *54*, 35−53.
(38) Kyoto University Phonon Database; http://phonondb.mtl.kyoto-u.ac.jp/ph20151124/index.html. 2015.

DOI: 10.1021/acsami.9b01242
ACS Appl. Mater. Interfaces XXXX, XXX, XXX−XXX